University of Nebraska - Lincoln

DigitalCommons@University of Nebraska - Lincoln

Nutrition and Health Sciences -- Faculty Publications

Nutrition and Health Sciences, Department of

2019

Urolithin A, a Gut Metabolite, Improves Insulin Sensitivity through Augmentation of Mitochondrial Function and Biogenesis

Ashley Mulcahy Toney

Rong Fan

Yibo Xian

Virginia Chaidez

Amanda E. Ramer-Tait

See next page for additional authors

Follow this and additional works at: https://digitalcommons.unl.edu/nutritionfacpub

Part of the Analytical, Diagnostic and Therapeutic Techniques and Equipment Commons, Enzymes and Coenzymes Commons, Human and Clinical Nutrition Commons, Molecular, Genetic, and Biochemical Nutrition Commons, and the Other Nutrition Commons

Authors

Ashley Mulcahy Toney, Rong Fan, Yibo Xian, Virginia Chaidez, Amanda E. Ramer-Tait, and Soonkyu Chung

Supplemental material follows the references.

Urolithin A, a Gut Metabolite, Improves Insulin Sensitivity through Augmentation of Mitochondrial Function and Biogenesis

Ashley Mulcahy Toney,[1] Rong Fan,[1] Yibo Xian,[2] Virginia Chaidez,[1]

Amanda E. Ramer-Tait,[2] and Soonkyu Chung,[1]

1. Department of Nutrition and Health Sciences, University of Nebraska–Lincoln, Lincoln, Nebraska, USA
2. Department of Food Science and Technology, University of Nebraska–Lincoln, Lincoln, Nebraska, USA

Corresponding author – Soonkyu Chung, email schung4@unl.edu

Abstract

Objective: Urolithin A (UroA) is a major metabolite of ellagic acid produced following microbial catabolism in the gut. Emerging evidence has suggested that UroA modulates energy metabolism in various cells. However, UroA's physiological functions related to obesity and insulin resistance remain unclear. *Methods:* Male mice were intraperitoneally administrated either UroA or dimethyl sulfoxide (vehicle) along with a high-fat diet for 12 weeks. Insulin sensitivity was evaluated via glucose and insulin tolerance tests and acute insulin signaling. The effects of UroA on hepatic triglyceride accumulation, adipocyte size, mitochondrial DNA content, and proinflammatory gene expressions were determined. The impact of UroA on macrophage polarization and mitochondrial respiration were assessed in bone marrow–derived macrophages. *Results:* Administration of UroA (1) improved systemic insulin sensitivity, (2) attenuated triglyceride accumulation and elevated mitochondrial biogenesis in the liver, (3) reduced adipocyte hypertrophy and macrophage infiltration into the adipose tissue, and (4) altered M1/M2 polarization in peritoneal macrophages. In addition, UroA favored macrophage M2 polarization and mitochondrial respiration in bone marrow–derived macrophages. *Conclusions:* UroA plays a direct role in improving systemic insulin sensitivity independent

of its parental compounds. This work supports UroA's role in the metabolic benefits of ellagic acid–rich foods and highlights the significance of its microbial transformation in the gut.

Introduction

The gut microbiota play a crucial role in host metabolism by enhancing energy extraction, generating signaling molecules such as short chain fatty acids, and modulating immune function (1). Moreover, gut microbes are involved in numerous catabolic pathways that can either intensify or annul the biological functions of dietary bioactive molecules. For example, gut microbial metabolism of dietary polyphenols could explain how these compounds exert an array of health benefits against obesity and its associated metabolic complications (2). Unfortunately, most polyphenolic compounds are notorious for their low bioavailability (3). A better understanding of how microbial catabolism in the gut generates bioavailable metabolites may one day aid in increasing the systemic levels of these compounds to mediate beneficial metabolic effects.

Urolithins (Uro) are one of the most extensively studied gut metabolites generated from ellagitannins (ET) and the free form of ellagic acid (EA). Uro possess a common 6H-dibenzo[*b*,*d*]-pyran-6-one nucleus and decreasing number of phenolic hydroxyl groups (UroD → UroC → UroA → UroB) following a series of microbial enzymatic actions in the gut (4) (Figure 1A). On intestinal absorption, Uro were shown to undergo phase II biotransformation in the liver, resulting in conjugated UroA metabolites, such as UroA-glucuronide and UroA-aglycone to a lesser amount (5). A recent study by Sandhu et al. demonstrated concentrations of UroA-glucuronide in human plasma around 0.142 μM to 5.96 μM 2 hours after chronic consumption of strawberry drink (6). In an extensive review, Tomás-Barberan et al. cited several studies reporting that UroA-glucuronide can be found at concentrations ranging from 0.024 μM to 35 μM in human plasma (7). However, these concentrations were shown to be highly dependent on the gut microbial composition of the host (8).

Despite numerous studies on pharmacokinetic production of UroA in the gut and its biological fate determination (7), less information is available on the physiological functions of Uro or the bioactive conjugates. Cerda et al. first proposed the hypothesis that Uro drive the health effects of ET and EA-containing foods (9). Afterward, a growing body of evidence has indicated that Uro convey metabolic benefits of EA-rich foods (10). In pioneering these efforts, Larrosa et al. reported that dietary administration of synthetic UroA (15 mg/kg of body weight (BW)/d) was effective in attenuating the colonic inflammation in a rat model, identifying the UroA could be a key anti-inflammatory metabolite derived from pomegranate extract (11). This anti-inflammatory role of UroA was confirmed in human colonic fibroblasts (12). Notably, the biological activities of UroA are found in various cell types beyond the site of UroA production and absorption in colorectal cells. Several *in vitro* studies have demonstrated the anti-inflammatory and antioxidative characteristics of UroA in immune, endothelial, and aortic cells (13–16). We demonstrated that UroA attenuated triglyceride (TG) accumulation in the primary human adipocytes (17). Recently, Ryu et al. demonstrated that UroA exhibited the unique function in promoting autophagic flux,

which led to increased longevity in *Caenorhabditis elegans* (18). Additionally, several studies demonstrated cardioprotective roles for UroA (19,20).

The aforementioned studies led us to hypothesize that UroA exerts the systemic metabolic benefits independent of its parental compounds EA or ET. To investigate the direct biological activities of UroA on lipid metabolism and insulin sensitivity, we employed a daily intraperitoneal (i.p.) injection of UroA in a physiologically relevant concentration (20 μg/mice). We reasoned that i.p. injection (1) bypasses the gastrointestinal tract, thereby avoiding redundant microbial catabolism of UroA, and (2) prompts the entry of the substance directly through the portal vein followed by hepatic first-pass metabolism before reaching systemic circulation (21). Here, we report that UroA injection mediates the enhanced insulin sensitivity against a high-fat (HF) diet. Our results support the direct biological function of UroA in modulating systemic insulin sensitivity and emphasize the metabolic significance of this gut-derived EA metabolite.

Methods

UroA preparation

UroA was obtained as described elsewhere (22). The stock consisted of 20 mg of UroA diluted in 5 mL of dimethyl sulfoxide (DMSO). This stock solution was freshly diluted with phosphate-buffered saline (PBS) (1:20) prior to use, and the final concentration of the UroA injection consisted of 20 μg per mouse, with the final DMSO blood concentration adjusted to < 0.3%. Control mice received the same volume of DMSO.

Animals

All animal procedures were approved by the Institutional Animal Care and Use Committee at the University of Nebraska–Lincoln. C57BL/6 male mice (Jackson Laboratory, Bar Harbor, Maine) were fed a HF diet *ad libitum*. The AIN-93 M purified rodent formulation was modified for fat composition consisting of 45% of the kilocalories from fat. All diet ingredients were purchased from Dyets, Inc. (Bethlehem, Pennsylvania). Mice were injected with either 100 μL vehicle ($n = 8$) or UroA ($n = 8$) daily for 12 weeks. BW change was monitored weekly. A glucose tolerance test (GTT) was performed on overnight-fasted mice by i.p. injection of 10% D-glucose (0.5 g/kg BW) (MilliporeSigma). Blood glucose levels were measured at 0, 30, 60, and 120 minutes post injection using a glucometer (Bayer Contour; Ascensia Diabetes Care, Basel, Switzerland). Blood was collected at 30 minutes post glucose injection during the GTT to measure insulin levels by enzyme-linked immunosorbent assay (ELISA) (Crystal Chem, Elk Grove Village, Illinois). An insulin tolerance test (ITT) was conducted 1 week after the GTT by injecting 1 U/kg human insulin (Novolin R; Novo Nordisk, Plainsboro, New Jersey). To study insulin signaling, mice ($n = 4$ per group) were fasted for 6 hours prior to i.p. injection of 1 U/kg human insulin. Liver and adipose tissues were collected at 15 minutes post insulin injection, and tissues were snap-frozen in liquid nitrogen and kept frozen until the assay. Peritoneal macrophages were collected from the peritoneal cavity and pooled for quantitative polymerase chain reaction (qPCR) analysis.

Cell culture

To obtain bone marrow–derived macrophages (BMDM), primary bone marrow was isolated from femurs and tibias from 5-week-old C57BL/6 mice as previously described (23). To investigate the role of UroA in macrophage polarization, BMDM were pretreated with either 30μM UroA or vehicle control (DMSO) in Opti-MEM (Gibco; Thermo Fisher Scientific, Waltham, Massachusetts) for 12 hours. To induce M1 polarization, BMDM were stimulated with lipopolysaccharide (LPS) (100 ng/mL) for 3 hours. To induce M2 macrophage polarization, medium containing interleukin (IL)-4 (100 ng/mL) and IL-13 (10 ng/mL) was added to the BMDM for 24 hours. The human hepatoma Huh7 cells were seeded at 2.5×10^5 cells per well in a six-well plate. At 70% confluence, cells were pretreated with 30μM UroA for 12 hours. To induce lipid accumulation, 400μM bovine serum albumin (BSA)-complex palmitic acid was added for 12 hours. BSA was used as negative control.

Measurement of oxygen consumption rate

BMDM underwent a Mito Stress Test to measure oxygen consumption rate (OCR) for basal and maximal respiration and ATP production using a Seahorse XFe24 extracellular flux analyzer (Agilent, Santa Clara, California). BMDM were cultured in a gelatin-coated Seahorse microplate (~12.5×10^4 cells/well). After pretreatment with 30μM UroA, BMDM were treated with IL-4 (100 ng/mL) and IL-13 (10 ng/mL) for M2 polarization for 24 hours. The cells were then treated with oligomycin (1μM) to measure ATP turnover. The maximum respiratory capacity was assessed by addition of carbonyl cyanide 4-trifluoromethoxyphenylhydrazone (FCCP) (0.3μM), a chemical uncoupler of electron transport and oxidative phosphorylation. Mitochondrial respiration was blocked by antimycin A (1μM) plus rotenone (1μM). OCR was calculated by plotting the O_2 tension of the medium in the microenvironment above the cells as a function of time (picomoles O_2 per minute). The extracellular acidification rate was calculated by measuring the acidity of the medium as a function of time (mpH per minute).

Liver TG quantification and blood biochemical parameters

A colorimetric TG quantification kit (Biovision, Milpitas, California) was used to quantify plasma and hepatic TG content according to the manufacturer's protocol. Total and low-density lipoprotein cholesterol (Abcam, Cambridge, UK) and nonesterified free fatty acids were measured using enzymatic kits (Wako Diagnostics, Richmond, Virginia). Plasma levels of adiponectin levels were quantified by commercial ELISA kit (R&D Systems, Minneapolis, Minnesota).

Hematoxylin and eosin staining and adipocyte size analysis

During necropsy, sections of the liver and epididymal white adipose tissue (eWAT) were immediately fixed (10% formalin), embedded in paraffin, cut to 10-μm sections, and processed for hematoxylin and eosin (H&E) staining. Adipocyte size was quantified using ImageJ and Adiposoft software (NIH, Bethesda, Maryland) (24).

Mitochondrial DNA quantification by qPCR

Liver and eWAT were analyzed for their mitochondrial DNA (mtDNA)/nuclear DNA (nDNA) ratio. Briefly, ~50 mg of liver and eWAT was homogenized using DNAzol Reagent (Invitrogen, Thermo Fisher Scientific), and the supernatant was retrieved. Quantitative reverse transcription PCR (qRT-PCR) was performed in duplicate using mtDNA-specific primers (16S ribosomal RNA) and nuclear-specific primers (hexokinase 2).

qRT-PCR

Gene-specific primers for qRT-PCR were obtained from Integrated DNA Technologies (Coralville, Iowa). Total RNA was isolated using TRIzol Reagent (Invitrogen). Gene expression was determined by real-time qPCR (ABI 7300, Applied Biosystems, Foster City, California), and relative gene expression was determined based on the $2^{-\Delta\Delta CT}$ method with normalization of the raw data to *18S* ribosomal RNA or hypoxanthine-guanine phosphoribosyltransferase (*Hprt*). The primer sequences for qPCR are available in Supplemental Table S1.

Western blot analysis

Tissues were homogenized in radioimmunoprecipitation assay buffer containing protease inhibitors (MilliporeSigma, Burlington, Massachusetts) and phosphatase inhibitors (2mM Na_3VO_4, 20mM β-glycerophosphate, and 10mM NaF). Proteins were fractionated using 10% to 12% sodium dodecyl sulfate (SDS) polyacrylamide gel electrophoresis (PAGE), transferred to polyvinylidene fluoride or polyvinylidene difluoride membranes, and incubated with the relevant antibodies. Chemiluminescence solution (Western Lightning; PerkinElmer, Waltham, Massachusetts) was detected using a FluorChem E imaging system (Cell Biosciences, Palo Alto, California). The sources of antibodies used in this work are listed in Supplemental Table S2.

Statistical analysis

Results are presented as mean ± SEM. The data were statistically analyzed by *t* test or one-way analysis of variance (ANOVA) with Tukey multiple comparison tests. All analyses were performed with GraphPad Prism 5 (version 5.04; GraphPad Software, San Diego, California).

Results

UroA improved insulin sensitivity in mice

To evaluate the role of UroA in modulating insulin sensitivity *in vivo*, mice were injected daily with UroA (20 μg/d) or DMSO (vehicle) for 12 weeks during HF diet feeding (Figure 1B). Although there was no difference in BW, UroA injection significantly improved the plasma lipid profile by decreasing total and low-density lipoprotein cholesterol levels. However, UroA showed no significant impacts on high-density lipoprotein cholesterol, plasma TG, and nonesterified free fatty acid content (Table 1). To investigate the effects of UroA on insulin sensitivity, we first conducted a GTT and ITT. HF+UroA mice displayed faster disposal of plasma glucose compared with HF mice (Figure 1C). Despite no differences in glucose levels at 30 minutes post glucose injection, HF+UroA mice maintained

lower insulin levels than HF mice, confirming their augmented insulin sensitivity. Similarly, HF+UroA mice were significantly more insulin sensitive compared with HF-fed mice during the ITT (Figure 1E). Next, we investigated the effects of UroA on insulin signaling in response to acute insulin challenge (1 U/kg). The phosphorylation status of the downstream targets of insulin (i.e., p-serine/threonine kinase 1 [Akt] and p-insulin receptor substrate 1 [IRS-1]) were significantly higher in HF+UroA mice than HF control mice both in the liver and adipose tissue (Figure 1F). Taken together, these results demonstrate that UroA exerts a direct role in improving insulin sensitivity in both the liver and adipose tissue independently of its parental compounds.
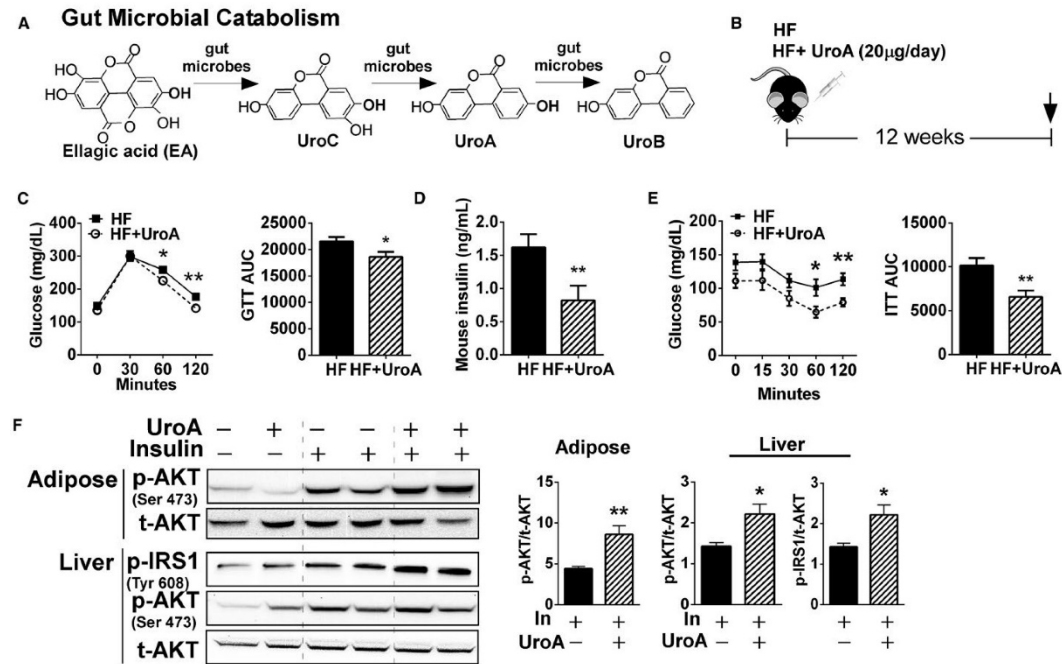

Figure 1. UroA injection increased insulin sensitivity in C57BL/6 mice against HF diet. (A) Production of Uro by gut microbes from EA. (B) Experimental scheme for UroA injection for 12 weeks. (C) Glucose tolerance test (GTT) and its area under the curve (AUC). (D) Insulin levels measured by ELISA at 30 minutes during GTT. (E) Insulin tolerance test and AUC. (F) Protein expression pattern for insulin signaling upon acute insulin injection (1 U/kg BW). All values represented as mean ± SEM (n = 8 per group). Phosphorylated (p)-Akt (Ser 473), p-IRS-1 (Tyr 608), and total (t)-Akt in the adipose and liver (left) from n = 4 per group. Relative protein intensities normalized to β-actin quantified by ImageJ (right). *$P < 0.05$ and **$P < 0.01$ by t test.

Table 1. Phenotype and blood lipid profiles

	HF ($n = 8$)	HF+UroA ($n = 8$)	*P* value
Phenotypes			
BW (g)	37.7 ± 1.40	35.7 ± 1.57	0.3540
Blood chemistry			
Total cholesterol (mg/dL)	164.8 ± 11.00	127.8 ± 11.43*	0.0379
HDL (mg/dL)	129.4 ± 2.77	130.7 ± 6.10	0.8338
LDL (mg/dL)	11.1 ± 0.54	7.3 ± 0.41***	0.0002
NEFA (mmol/L)	0.62 ± 0.05	0.55 ± 0.06	0.3982
Triglycerides (mmol/L)	0.99 ± 0.05	0.89 ± 0.08	0.3404
Adiponectin (μg/dL)	12.9 ± 0.87	18.1 ± 1.27**	0.0073

Values are mean ± SEM.

*$P < 0.05$ by *t* test.

**$P < 0.01$ by *t* test.

***$P < 0.001$ by *t* test.

BW, body weight; HDL, high-density lipoprotein; LDL, low-density lipoprotein; NEFA, nonesterified free fatty acids.

UroA decreased hepatic TG accumulation and inflammation

Previously, we demonstrated that UroA decreased TG accumulation in human hepatocytes (17). To determine whether UroA injection recapitulates these results *in vivo*, we investigated hepatic TG regulation. UroA treatment did not induce any apparent morphological changes in the liver compared with control mice (data not shown). To confirm whether UroA causes phase I drug metabolism, we examined transcript levels of *Cyp2e1*, a cytochrome P450 dependent oxidase responsible for the detoxification of xenobiotics. There were no differences in *Cyp2e1* levels between treatments, suggesting that UroA injection (20 μg/d) does not cause hepatic toxicity (Figure 2A). Although liver tissue weight was not significantly different between treatments, an analysis of hepatic TG showed a significant decrease in TG levels in HF+UroA mice compared with mice fed HF alone (Figure 2B). H&E staining of the liver tissue revealed that TG accumulation was significantly lower in HF+UroA mice than HF mice (Figure 2C). Corroborating this, liver tissue from HF+UroA had decreased levels of lipogenic gene and protein expression (e.g., fatty acid synthase [FASN], stearoyl-CoA desaturase 1 [SCD1]) but significantly increased expression of beta-oxidation genes (carnitine palmitoyltransferase 1 [*Cpt1*] and sirtuin 1 [*Sirt1*]) (Figure 2D–2E). Moreover, livers from HF+UroA mice had augmented expression of reactive oxygen species-quenching related genes, such as superoxide dismutase 1 (*Sod1*) and 2 (*Sod2*) (Figure 2D). Lastly, both *Il1b* expression (Figure 2D) and nuclear factor-κB (NFκB) inhibitor alpha (IκBα) degradation (Figure 2F) were significantly decreased in HF+UroA liver tissue, suggesting the attenuation of NFκB activation by UroA. Consistent with reduced hepatic steatosis, livers from HF+UroA mice had significantly reduced levels of the endoplasmic reticulum stress markers of phosphorylated mitogen-activated protein kinase 8 (p-JNK), eukaryotic translation initiation factor 2A (p-EIf2α), and mitogen-activated protein kinase 1 (p-ERK) (Figure 2F). Also, UroA increased microtubule associated protein 1 light chain 3 (LC3II) accumulation, indicating elevated autophagy in the livers of UroA-

injected mice (Figure 2F). Notably, the mtDNA/nDNA ratio was significantly elevated in HF+UroA livers (P = 0.002), indicating augmented mitochondrial biogenesis (Figure 2E). These results were validated in human hepatoma Huh7 cells. Consistent with our previous study (17), treatment of Huh7 cells with 30μM UroA reduced palmitate-induced TG accumulation compared with the vehicle control, as shown in oil red O staining (Figure 2G). Moreover, lipogenic gene expression, including sterol regulatory element binding transcription factor 1 (*Srebp1c*), *Fasn*, *Scd1*, acetyl-CoA carboxylase (*Acc*), and diacylglycerol O-acyltransferase 2 (*Dgat2*), was significantly decreased in UroA-treated Huh7 cells (Figure 2H). Simultaneously, genes related to mitochondrial fatty acid oxidation (i.e., *Cpt1* and *Sirt1*) were significantly increased (Figure 2H), and Il-1β was dramatically decreased in UroA-treated Huh7 cells (Figure 2H). Taken together, these results suggest that augmented mitochondrial activity and mass contribute to the TG-lowering effects of UroA.
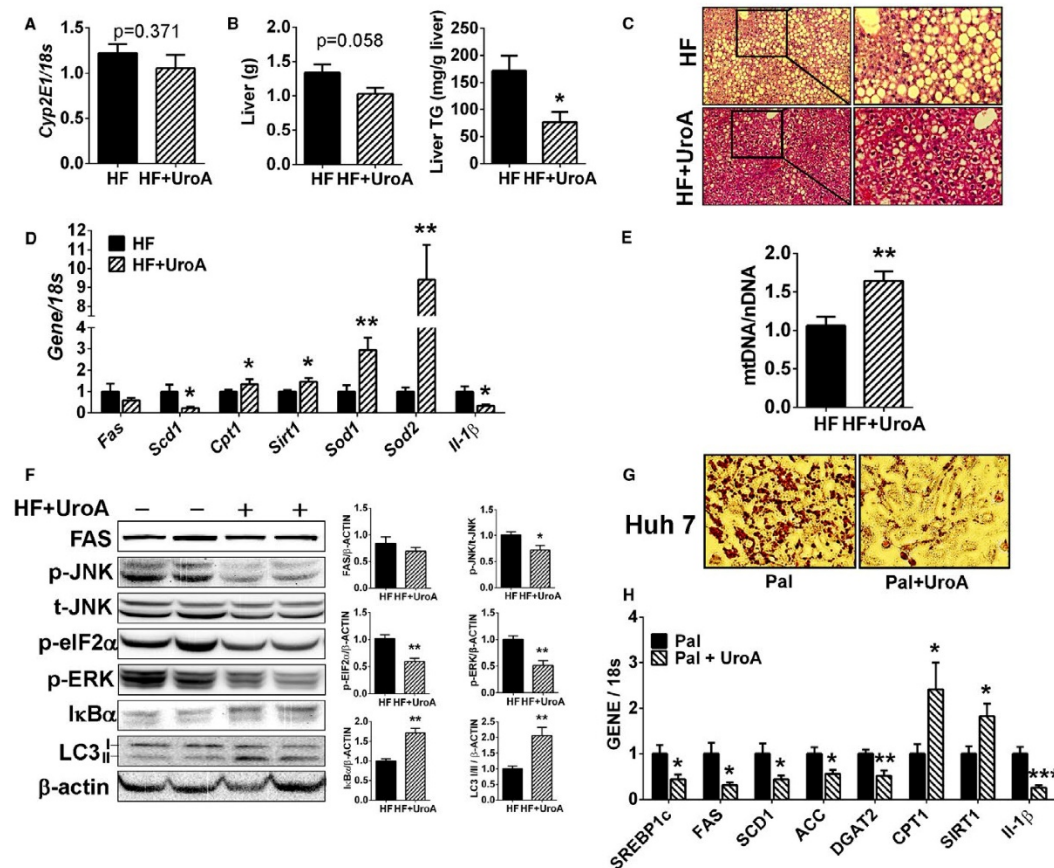

Figure 2. UroA attenuated hepatic TG accumulation and inflammation. (A-F) C57BL/6 mice were fed a HF diet and given a daily injection of either UroA or DMSO for 12 weeks (*n* = 8 per group). (A) *Cyp2e1* transcript levels by qPCR. (B) Liver weight (grams) and hepatic TG content (milligrams/gram liver). (C) H&E staining of liver tissues. (D) Hepatic gene expression levels measured by qPCR; *Fasn* and *Scd1* (de novo lipogenesis), *Cpt1* and *Sirt1* (beta-oxidation), *Sod1* and *Sod2* (reactive oxygen species quenching), and *Il1b*

(inflammation). (E) Relative mtDNA to nDNA in the liver ($n = 5$). (F) Protein expression patterns of FASN, p-eIF2α, p-ERK, IκBα, and LC3I/II by Western blot analysis. Relative protein intensities normalized to β-actin quantified by ImageJ (right). (G–H) Huh7 hepatoma cells pretreated with either 30μM UroA or DMSO followed by stimulation with palmitic acid (400μM). (G) TG accumulation in Huh7 cells by oil red O staining. (H) Gene expression levels of *Srebp1c*, *Fasn*, *Scd1*, *Acc*, and *Dgat2* (lipogenesis); *Cpt1* and *Sirt1* (fatty acid oxidation), and *Il1b* (inflammation) in Huh7 cells. All values represented as mean ± SEM. *$P < 0.05$, **$P < 0.01$, and ***$P < 0.001$ by *t* test.

UroA decreased adipocyte hypertrophy and macrophage infiltration in adipose tissue

Our laboratory has previously demonstrated the role of UroA in reducing lipogenesis by using primary cultures of human adipocytes *in vitro* (17). In this study, we collected eWAT from mice to validate the physiological function of UroA in adipose tissue. UroA injection tended to decrease eWAT mass (Figure 3A) and noticeably reduced adipocyte size as revealed by H&E staining. A quantitative analysis of adipocyte size and distribution confirmed our observation of reduced hypertrophy following UroA treatment (Figure 3C–3D). In agreement with the reduced adipose hypertrophy, FASN and ACC levels were reduced, while peroxisome proliferator-activated receptor gamma (PPARγ) expression was higher in UroA-treated mice (Figure 3E). The smaller adipocyte size induced by UroA injection also correlated with increased adiponectin gene (*Adipoq*) expression (Figure 3F) and plasma levels (Table 1).

Of note, we observed increased expression of PPARγ coactivator 1 alpha (*Pgc1a*; also known as *Ppargc1a*) and *Sirt1* mRNA in UroA-treated eWAT (Figure 3F), implicating increased mitochondrial biogenesis. UroA treatment increased the expression of mitochondrial-specific proteins in eWAT, including voltage-dependent anion-selective channel protein (VDAC) (mitochondrial outer membrane) and pyruvate dehydrogenase (matrix) (PDH) (Figure 3G). This observation was further confirmed by an increased mtDNA/nDNA ratio in UroA-treated eWAT compared with DMSO controls (Figure 3H). Next, we examined whether UroA reduces macrophage infiltration into eWAT, as adipocyte hypertrophy is associated with inflammation (25). Both gene and protein levels of *Mcp1* and *F4/80* were reduced following UroA injection (Figure 3F–3G). In addition, expression of CD11c also known as integrin alpha X (ITGAX), a proinflammatory M1 macrophage marker, was also drastically reduced (Figure 3G). Collectively, these results not only confirm the ability of UroA to reduce adipocyte hypertrophy but also reveal a previously unidentified role of UroA in decreasing macrophage infiltration and promoting mitochondrial biogenesis in eWAT.
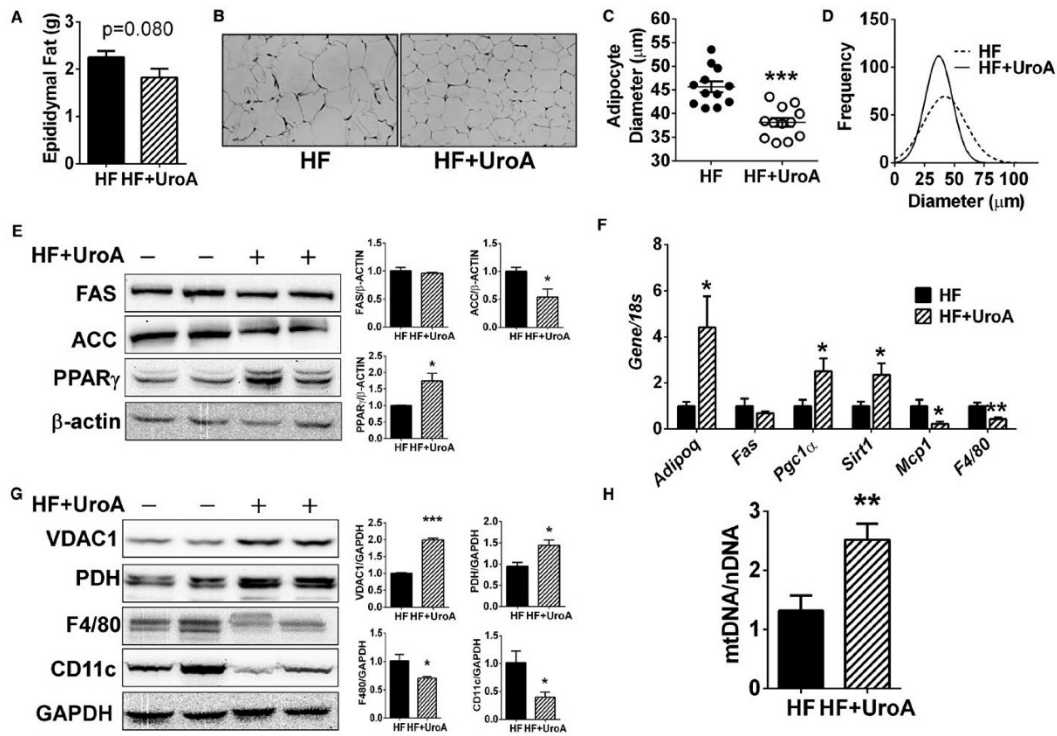
Figure 3. UroA decreased adipocyte hypertrophy and macrophage infiltration. eWAT was harvested after daily injection of either UroA or DMSO for 12 weeks ($n = 8$ per group). (A) eWAT weight (gram, $n = 8$). (B) H&E staining of eWAT. (C) Average adipocyte diameter (micrometers) by ImageJ. (D) Adipocyte size distribution. Line of best fit is shown (Gaussian curve fitting). (E) Protein expression pattern of FASN, ACC, and PPARγ in eWAT. Relative protein intensities normalized to β-actin quantified by ImageJ (right). (F) Gene expression levels of *Adipoq* and *Fasn*, *Pgc1a*, and *Sirt1*, *Mcp1*, and *F4/80* by qPCR. (G) Protein expression pattern of VDAC1 and PDH (mitochondrial proteins) and F4/80 and CD11c (macrophage markers) by Western blot analysis. Relative protein intensities normalized to glyceraldehyde-3-phosphate dehydrogenase (GAPDH) quantified by ImageJ (right). (H) mtDNA to nDNA ratio in eWAT by qPCR. All values represented as mean ± SEM. *$P < 0.05$, **$P < 0.01$, and ***$P < 0.001$ by t test.

UroA altered M1/M2 polarization in peritoneal macrophages

Because UroA decreases macrophage infiltration into adipose tissue, we examined the in-flammatory status of peritoneal macrophages (Mϕ) harvested from HF and HF+UroA mice. We observed a remarkable decrease in proinflammatory M1 Mϕ markers, including *Cd11c*, tumor necrosis factor (*Tnfα*), *Il6*, *Il1b*, and *Mcp1* (Figure 4A). Conversely, the resolv-ing M2 phenotype markers chitinase-like 3 (*Ch3l3*; also known as *Chil3*) and macrophage galactose N-acetyl-galactosamine specific lectin 2 (*Mgl2*) were significantly increased in peritoneal Mϕ (Figure 4A). To confirm the role of UroA in M1/M2 polarization, we pre-treated primary BMDM with UroA. Such treatment significantly decreased *Il1b* and *Tnfα* expression in response to LPS stimulation (Figure 4B). In agreement with our *in vivo* re-sults, UroA markedly enhanced M2 Mϕ markers of arginase, liver (*Arg1*), *Chil3*, and *Mgl2* in pretreated BMDM subsequently stimulated with IL-4 and IL-13 (Figure 4C). We next sought to determine the mitochondrial respiration rate of M2 polarized BMDM as a meas-ure of UroA's impact on macrophage metabolism. OCR was higher in M2 polarized BMDM than nonpolarized control Mϕ. Importantly, UroA pretreatment further promoted OCR for both basal and ATP production (Figure 4D). In parallel to enhanced mitochondrial respiration, the rank order of extracellular acidification rate in BMDM was unstimulated Mϕ > M2 Mϕ > M2+UroA Mϕ, indicating that UroA drives decreased anaerobic respiration in BMDM via alterations in glycolysis (Figure 4D). Collectively, these results uncover a previously unappreciated role of UroA in favoring M2 polarization of macrophages, thereby mediating attenuated inflammation and improving insulin sensitivity.
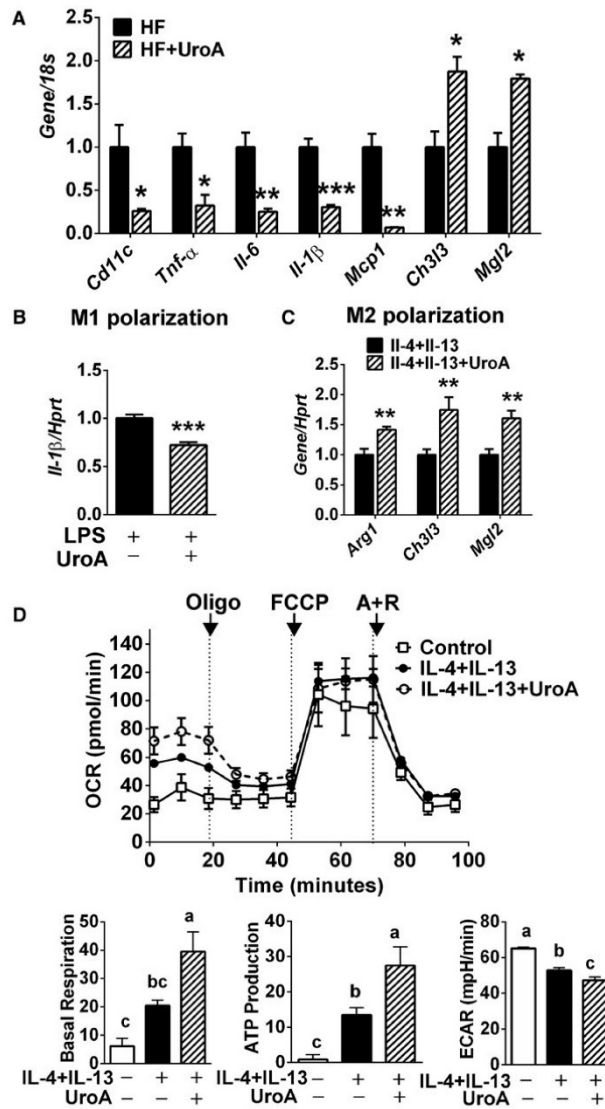
Figure 4. UroA favored M2 polarization in macrophages. (A) Peritoneal macrophages were collected after chronic injection with UroA for 12 weeks, and (B–D) BMDM from naïve mice were treated with UroA (30μM). (A) Gene expression levels in macrophages by qPCR; *Cd11c*, *Tnf-α*, *Il6*, *Il1b*, and *Mcp1* (M1 markers) and *Ch3l3* and *Mgl2* (M2 markers). (B) *Il1b* expression after LPS stimulation for 3 hours in BMDM. (C) Gene expression of *Arg1*, *Ch3l3*, and *Mgl2* (M2 markers) in BMDM after stimulation with IL-4 plus IL-13. (D) Mitochondrial OCR by extracellular flux analyzer (*n* = 5). Basal respiration rate and ATP production and extracellular acidification rate. Arrows indicate the addition of the respiratory inhibitor oligomycin (Oligo), FCCP, and antimycin A plus rotenone (A+R). All values represented as mean ± SEM. *$P < 0.05$, **$P < 0.01$, and ***$P < 0.001$ by *t* test. Treatments with different letters are significantly different from one another ($P < 0.05$) by one-way ANOVA.

Discussion

Previous studies have demonstrated compelling biological activities at the cellular level of UroA, a first-in-class natural compound derived from EA (7); however, its systemic metabolic functions remain unclear. Our current study aims to assess the independent role of UroA in modulating both insulin resistance and meta-inflammation in dietary challenge with a HF diet. We demonstrated that UroA injection through the i.p. route (1) alleviated HF diet–related insulin resistance (Figure 1), (2) attenuated hepatic TG accumulation and adipocyte hypertrophy (Figures 2 and 3), (3) reduced hepatic and adipose inflammation (Figures 2 and 3), and (4) conferred resistance to HF diet–mediated M1 polarization of macrophages (Figure 4). Our study reveals a novel mechanism by which UroA improves metabolic profiles via augmentation of mitochondrial activities and biogenesis in the liver and adipose tissue and through promoting macrophage M2 differentiation.

In this pilot study, we administrated 20 μg of UroA via i.p. injection, which is roughly equivalent to 0.8 mg/kg per mouse per day of free UroA. When we calculated the human equivalent dose by applying the scaling factor of 12.3 (26), the estimated value was 0.065 mg/kg per human per day. For a 60-kg adult human, roughly ~3.9 mg of free UroA or ~7.0 mg of UroA-glucuronide should exist in circulation to predict similar biological effects found in HF-fed mice. Although ~7 mg of UroA-glucuronide in the bloodstream (3.6μM in plasma assuming 8% of blood volume in a 60-kg adult human) seems challenging, it is attainable in human plasma because 0.024μM to 35μM UroA-glucuronide could be found in human plasma after ingestion of EA-rich fruit juice (7).

UroA metabolites in plasma undergo rapid clearance, but turnover kinetics is not well known. Most studies have measured the UroA plasma concentration within a maximum 6-hour post ingestion time frame (6,27). However, this post ingestion time frame seems to be valid only after chronic ingestion. Recently, Istas et al. showed that UroA metabolites showed up in plasma in the form of glucuronide or sulfate after 24-hour intake of 200 g to 400 g of whole red raspberry (28). Unfortunately, we failed to collect plasma and tissue samples in an earlier time frame. Our efforts to quantify the UroA metabolites in the plasma and tissue samples collected after 24 hours of UroA injection were unsuccessful (only trace amounts of UroA metabolites were detected in the adipose tissue). The lack of information regarding the concentration and molecular form of circulatory UroA is a caveat in our study. Regardless, this information provides evidence for immediate bioconversion of i.p.-administered and insoluble UroA into bioavailable UroA metabolites (presumably glucuronidation in the liver), as no detectable UroA precipitates occur in the plasma or accumulate in peripheral tissues.

In term of toxicity, it is far below the no-observed-adverse-effect levels of UroA tested in rats for 90 days (3,451 mg/kg and 3,826 mg/kg of BW per day in male and female rats, respectively) (29). Consistent with this finding, we did not observe any phenotypic abnormalities in the livers of mice injected with UroA (data not shown), nor did we observe induction of phase I drug metabolism such as *Cyp2e1* activation (Figure 2A). Accumulating evidence has supported that UroA undergoes biotransformation in the liver through phase II conjugation (30,31). As a result, UroA-glucuronide is formed as the principal metabolite found in plasma, tissues, and urine over UroA-aglycone conjugates (7).

Either produced by gut microbial actions or chemically synthesized, UroA exerts pleiotropic effects in various cell types (7). Although metabolic findings do differ among studies, the following two underlying mechanisms are common and correlate with UroA-mediated health benefits: (1) activation of mitochondrial function and quality control and (2) suppression of proinflammatory signaling. Here, we discussed how these two underlying mechanisms fit with our findings that UroA improves insulin sensitivity via regulation of mitochondrial activities and inflammation.

One critical signal necessary for upregulation of mitochondrial activities is 5′-AMP-activated protein kinase (AMPK). Upon activation by a vast range of polyphenolic compounds, AMPK turns off anabolic pathways such as TG accumulation, but it turns on catabolic pathways such as beta-oxidation (32). A few studies have reported that consumption of EA-rich foods improves insulin sensitivity and attenuates lipid accumulation and inflammation through, at least in part, AMPK activation (17,33). Zhao et al. found that raspberries improved insulin sensitivity, lowered lipid accumulation and inflammation, and increased skeletal mitochondrial capacity in wild-type mice but not in AMPK^{-/-} mice (33). Previously, our labs demonstrated the direct role of UroA for AMPK phosphorylation and beta-oxidation when primary adipocytes and Huh7 cells were treated with UroA (17). In our current study, we observed reduced TG accumulation and increased beta-oxidation in both liver and adipose tissue (Figures 2 and 3). Unexpectedly, differences in AMPK activation were less evident (data are not shown), presumably because of the fasting status of the mice at the time of necropsy. Alternatively, we observed increased accumulation of LC3II, a sign for autophagic activation (Figure 2F), and mitochondrial biogenesis (Figure 2E) in livers from UroA-treated mice. The autophagy activation is linked with the removal of damaged organelles to maintain the cellular homeostasis including mitochondria (34). In support of this notion, emerging evidence has suggested that UroA promotes mitophagy in *C. elegans* and rat muscle (18), as well as in UroA-treated J774.1 macrophages (35). UroA promotion of mitochondrial biogenesis (Figure 2E) could be expected, as tight coordination was shown between mitophagy and mitochondrial biogenesis to maintain mitochondrial homeostasis (36). Collectively, our results demonstrate that UroA promotes mitochondrial activities by maintaining healthy mitochondrial homeostasis and mitochondrial biogenesis.

One unequivocal response we routinely observed upon UroA administration was the remarkable suppression of inflammation (13,37). In particular, we saw a significant reduction in the expression of proinflammatory markers, cytokines, and chemokines in liver, adipose, and macrophages of UroA-injected mice (Figures 2, 3, and 4). Because adipose inflammation plays a critical role in whole-body insulin resistance, UroA-induced insulin sensitivity (Figure 1) might result from the cumulative effects of UroA on adipose tissue by reducing hypertrophy (Figure 3C–3D, 3G), elevating adiponectin levels (Table 1), and inhibiting macrophage infiltration (Figure 3G). Importantly, our findings support a novel function of UroA in promoting M2 polarization. We demonstrated that UroA not only markedly decreased M1 polarization but also simultaneously increased M2 polarization *in vivo* (Figure 4A) and *in vitro* (Figure 4B–4C). Advances in immunometabolism have revealed that M2 Mϕ utilizes ATP from oxidative phosphorylation, whereas M1 Mϕ favors ATP from substrate-level phosphorylation during glycolysis (38). Conforming to this

metabolic switch, UroA further increased mitochondrial oxygen consumption (Figure 4D), a finding supported by Ryu et al. who showed increased aerobic capacity and OCR in skeletal muscle following UroA treatment (18). Taken together, our results indicate that UroA acts on macrophages to induce M2 differentiation, thereby contributing to the reduced inflammation and metabolic improvements.

The mode of action that UroA exerts for health benefits is reminiscent of resveratrol. Resveratrol was shown to activate SIRT1, a histone deacetylase (39). Previous studies showed that the parental compound of UroA, EA, modulated histone-arginine methylation (40). Consequently, future studies investigating whether UroA directly affects histone modifications may prove worthwhile. In addition, UroA may also exert an immediate effect on insulin signaling. Tang et al. found that UroA might directly target the phosphoinositide-3-kinase (PI3K)/Akt pathway in the primary neonatal rat myocardiocytes (20), suggesting that multiple signaling pathways could be involved in UroAmediated improvements in insulin sensitivity.

Conclusion

We demonstrated that UroA is capable of attenuating HF diet–induced obesity and insulin resistance. Here, we also identified a novel immune-modulatory role of UroA in macrophages that favor M2 polarization. Additionally, we observed that UroA regulates signaling pathways previously proposed to potentiate mitochondrial activities. Future studies should determine the active concentration range of UroA in the hepatic and peripheral tissues necessary to exert metabolic benefits. Furthermore, it should be evaluated whether oral consumption of UroA would be as effective as UroA injection. We believe our study builds on growing evidence of UroA's ability to increase mitochondrial respiration and sheds new light on the dietary strategy to boost this gut metabolite to circumvent obesity-mediated metabolic complications.

Disclosure: The authors declare no conflict of interest.

References

1. Rosenbaum M, Knight R, Leibel RL. The gut microbiota in human energy homeostasis and obesity. *Trends Endocrinol Metab* 2015; 26:493–501.
2. Roopchand DE, Carmody RN, Kuhn P, et al. Dietary polyphenols promote growth of the gut bacterium Akkermansia muciniphila and attenuate high-fat diet-induced metabolic syndrome. *Diabetes* 2015; 64:2847–2858.

3. Manach C, Scalbert A, Morand C, Rémésy C, Jiménez L. Polyphenols: food sources and bioavailability. *Am J Clin Nutr* 2004; 79:727–747.

4. Espín JC, Larrosa M, Garcia-Conesa M-T, Tomás-Barberán FA. Biological significance of urolithins, the gut microbial ellagic acid–derived metabolites: the evidence so far. *Evid Based Complement Alternat Med* 2013; 2013:15. doi:10.1155/2013/270418

5. González-Sarrías A, Azorín-Ortuño M, Yáñez-Gascón M-J, Tomás-Barberán FA, García-Conesa M-T, Espín J-C. Dissimilar in vitro and in vivo effects of ellagic acid and its microbiota-derived metabolites, urolithins, on the cytochrome P450 1A1. *J Agric Food Chem* 2009; 57:5623–5632.

6. Sandhu AK, Miller MG, Thangthaeng N, et al. Metabolic fate of strawberry polyphenols after chronic intake in healthy older adults. *Food Funct* 2018; 9:96–106.

7. Tomás-Barberán FA, González-Sarrías A, García-Villalba R, et al. Urolithins, the rescue of "old" metabolites to understand a "new" concept: metabotypes as a nexus among phenolic metabolism, microbiota dysbiosis, and host health status. *Mol Nutr Food Res* 2017; 61:1500901. doi:10.1002/mnfr.201500901

8. Selma MV, Gonzalez-Sarrias A, Salas-Salvado J, et al. The gut microbiota metabolism of pomegranate or walnut ellagitannins yields two urolithin-metabotypes that correlate with cardiometabolic risk biomarkers: comparison between normoweight, overweight-obesity and metabolic syndrome. *Clin Nutr* 2018; 37:897–905.

9. Cerda B, Tomas-Barberan FA, Espin JC. Metabolism of antioxidant and chemopreventive ellagitannins from strawberries, raspberries, walnuts, and oak-aged wine in humans: identification of biomarkers and individual variability. *J Agric Food Chem* 2005; 53:227–235.

10. Kang I, Buckner T, Shay NF, Gu L, Chung S. Improvements in metabolic health with consumption of ellagic acid and subsequent conversion into urolithins: evidence and mechanisms. *Adv Nutr* 2016; 7:961–972.

11. Larrosa M, Gonzalez-Sarrias A, Yanez-Gascon MJ, et al. Anti-inflammatory properties of a pomegranate extract and its metabolite urolithin-A in a colitis rat model and the effect of colon inflammation on phenolic metabolism. *J Nutr Biochem* 2010; 21:717–725.

12. Gonzalez-Sarrias A, Larrosa M, Tomas-Barberan FA, Dolara P, Espin JC. NFkappaB-dependent anti-inflammatory activity of urolithins, gut microbiota ellagic acid-derived metabolites, in human colonic fibroblasts. *Br J Nutr* 2010; 104:503–512.

13. Piwowarski JP, Kiss AK, Granica S, Moeslinger T. Urolithins, gut microbiota–derived metabolites of ellagitannins, inhibit LPS-induced inflammation in RAW 264.7 murine macrophages. *Mol Nutr Food Res* 2015; 59:2168–2177.

14. Spigoni V, Mena P, Cito M, et al. Effects on nitric oxide production of urolithins, gut-derived ellagitannin metabolites, in human aortic endothelial cells. *Molecules* 2016; 21:1009. doi:10.3390/molecules21081009

15. Piwowarski JP, Granica S, Kiss AK. Influence of gut microbiota-derived ellagitannins' metabolites urolithins on pro-inflammatory activities of human neutrophils. *Planta Med* 2014; 80:887–895.

16. Gimenez-Bastida JA, Gonzalez-Sarrias A, Larrosa M, Tomas-Barberan F, Espin JC, Garcia-Conesa MT. Ellagitannin metabolites, urolithin A glucuronide and its aglycone urolithin A, ameliorate TNF-alpha-induced inflammation and associated molecular markers in human aortic endothelial cells. *Mol Nutr Food Res* 2012;56:784–796.

17. Kang I, Kim Y, Tomas-Barberan FA, Espin JC, Chung S. Urolithin A, C, and D, but not isourolithin A and urolithin B, attenuate triglyceride accumulation in human cultures of adipocytes and hepatocytes. *Mol Nutr Food Res* 2016;60:1129–1138.

18. Ryu D, Mouchiroud L, Andreux PA, et al. Urolithin A induces mitophagy and prolongs lifespan in C. elegans and increases muscle function in rodents. *Nat Med* 2016;22:879–888.

19. Savi M, Bocchi L, Mena P, et al. In vivo administration of urolithin A and B prevents the occurrence of cardiac dysfunction in streptozotocin-induced diabetic rats. *Cardiovasc Diabetol* 2017;16:80. doi:10.1186/s12933-017-0561-3

20. Tang L, Mo Y, Li Y, et al. Urolithin A alleviates myocardial ischemia/reperfusion injury via PI3K/Akt pathway. *Biochem Biophys Res Comm* 2017;486:774–780.

21. Lukas G, Brindle SD, Greengard P. The route of absorption of intraperitoneally administered compounds. *J Pharmacol Exp Ther* 1971;178:562–564.

22. Garcia-Villalba R, Espin JC, Tomas-Barberan FA. Chromatographic and spectroscopic characterization of urolithins for their determination in biological samples after the intake of foods containing ellagitannins and ellagic acid. *J Chromatogr A* 2016;1428:162–175.

23. Zhao L, Kang I, Fang X, et al. Gamma-tocotrienol attenuates high-fat diet-induced obesity and insulin resistance by inhibiting adipose inflammation and M1 macrophage recruitment. *Int J Obes* 2015;39:438–446.

24. Galarraga M, Campión J, Muñoz-Barrutia A, et al. Adiposoft: an automated software for the analysis of white adipose tissue cellularity in histological sections. *J Lipid Res* 2012;53:2791–2796.

25. Ghigliotti G, Barisione C, Garibaldi S, et al. Adipose tissue immune response: novel triggers and consequences for chronic inflammatory conditions. *Inflammation* 2014;37:1337–1353.

26. Reagan-Shaw S, Nihal M, Ahmad N. Dose translation from animal to human studies revisited. *FASEB J* 2008;22:659–661.

27. Seeram NP, Henning SM, Zhang Y, Suchard M, Li Z, Heber D. Pomegranate juice ellagitannin metabolites are present in human plasma and some persist in urine for up to 48 hours. *J Nutr* 2006;136:2481–2485.

28. Istas G, Feliciano RP, Weber T, et al. Plasma urolithin metabolites correlate with improvements in endothelial function after red raspberry consumption: a double-blind randomized controlled trial. *Arch Biochem Biophys* 2018;651:43–51.

29. Heilman J, Andreux P, Tran N, Rinsch C, Blanco-Bose W. Safety assessment of Urolithin A, a metabolite produced by the human gut microbiota upon dietary intake of plant derived ellagitannins and ellagic acid. *Food Chem Toxicol* 2017;108(Pt A): 289–297.

30. Piwowarski JP, Stanislawska I, Granica S, Stefanska J, Kiss AK. Phase II conjugates of urolithins isolated from human urine and potential role of beta-glucuronidases in their disposition. *Drug Metab Dispos* 2017;45:657–665.

31. Gonzalez-Sarrias A, Gimenez-Bastida JA, Nunez-Sanchez MA, et al. Phase-II metabolism limits the antiproliferative activity of urolithins in human colon cancer cells. *Eur J Nutr* 2014;53:853–864.

32. Mihaylova MM, Shaw RJ. The AMPK signaling pathway coordinates cell growth, autophagy, and metabolism. *Nat Cell Biol* 2011;13:1016–1023.

33. Zhao L, Zou T, Gomez NA, Wang B, Zhu M-J, Du M. Raspberry alleviates obesity-induced inflammation and insulin resistance in skeletal muscle through activation of AMP-activated protein kinase (AMPK) α1. *Nutr Diabetes* 2018;8:39. doi:10.1038/s41387-018-0049-6

34. Kim KH, Lee MS. Autophagy—a key player in cellular and body metabolism. *Nat Rev Endocrinol* 2014;10:322–337.

35. Boakye YD, Groyer L, Heiss EH. An increased autophagic flux contributes to the anti-inflammatory potential of urolithin A in macrophages. *Biochim Biophys Acta* 2018;1862:61–70.

36. Palikaras K, Lionaki E, Tavernarakis N. Coordination of mitophagy and mitochondrial biogenesis during ageing in C. elegans. *Nature* 2015;521:525–528.

37. Komatsu W, Kishi H, Yagasaki K, Ohhira S. Urolithin A attenuates pro-inflammatory mediator production by suppressing PI3-K/Akt/NF-kappaB and JNK/AP-1 signaling pathways in lipopolysaccharide-stimulated RAW264 macrophages: possible involvement of NADPH oxidase-derived reactive oxygen species. *Eur J Pharmacol* 2018;833:411–424.

38. Galván-Peña S, O'Neill LAJ. Metabolic reprograming in macrophage polarization. *Front Immunol* 2014;5:420. doi:10.3389/fimmu.2014.00420

39. Lagouge M, Argmann C, Gerhart-Hines Z, et al. Resveratrol improves mitochondrial function and protects against metabolic disease by activating SIRT1 and PGC-1alpha. *Cell* 2006;127:1109–1122.

40. Kang I, Okla M, Chung S. Ellagic acid inhibits adipocyte differentiation through coactivator-associated arginine methyltransferase 1-mediated chromatin modification. *J Nutr Biochem* 2014;25:946–953.

Table S1. Primer sequences for qPCR

Gene	Forward/Reverse	Sequence (5′-3')
mAdiponectin	Forward	ACAATGGCACACCAGGCCGT
	Reverse	TGCCAGGGGTTCCGGGGAAG
mFas	Forward	GGAGGTGGTGATAGCCGGTAT
	Reverse	TGGGTAATCCATAGAGCCCAG
mScd1	Forward	GGGACAGATATGGTGTGAAACTATG
	Reverse	TTACAGACACTGCCCCTCAAC
mF4/80	Forward	CTTTGGCTATGGGCTTCCAGTC
	Reverse	GCAAGGAGGACAGAGTTTATCGTG
mCpt1	Forward	CCAGGCTACAGTGGGACATT
	Reverse	AAGGAATGCAGGTCCACATC
mSirt1	Forward	TCGTGGAGACATTTTTAATCAGG
	Reverse	GCTTCATGATGGCAAGTGG
mSod1	Forward	CGTACAATGGTGGTCCATGA
	Reverse	GTTTACTGCGCAATCCCAAT
mSod2	Forward	AACTCAGGTCGCTCTTCAGC
	Reverse	GCTTGATAGCCTCCAGCAAC
mIl-1b	Forward	AAATACCTGTGGCCTTGGGC
	Reverse	CTTGGGATCCACACTCTCCAG
mPgc1a	Forward	CCCTGCCATTGTTAAGACC
	Reverse	TGCTGCTGTTCCTGTTTTC
hSCD1	Forward	GGGTGAGGGCTTCCACAACTA
	Reverse	CGGCCATGCAATCAATGAA
hSREBP1c	Forward	TGC ATT TTC TAG CAC GCT TC
	Reverse	GAT GTT CCC GGA ATA GCT GA
hFAS	Forward	GGCAAGCTGAAGGACCTGTCTA
	Reverse	AATCTGGGTTGATGCCTCCGT
hACC	Forward	CATCAAATGCATCAGCAGAGACT
	Reverse	CTGCGTCATATGGATGATGGAAT
hDGAT2	Forward	TCCAGCTGGTGAAGACACAC
	Reverse	TCACTTCTGTGGCCTCTGTG
hCPT1	Forward	CTTTGGCCCTGTAGCAGATGA
	Reverse	TCGTCTCTGAGCTTGAGAACTT
hSIRT1	Forward	CGGAAACAATACCTCCACCT
	Reverse	CACCCCAGCTCCAGTTAGAA
hIL-1b	Forward	GCCCTAAACAGATGAAGTGCTC
	Reverse	GAACCAGCATCTTCCTCA
mMcp1	Forward	AGGTCCCTGTCATGCTTCTG
	Reverse	GCTGCTGGTGATCCTCTTGT

mCd11c	Forward	CTGGATAGCCTTTCTTCTGCTG
	Reverse	GCACACTGTGTCCGAACTC
mTnfa	Forward	GGCTGCCCCGACTACGT
	Reverse	ACTTTCTCCTGGTATGAGATAGCAAAT
mIl-6	Forward	CTGCAAGAGACTTCCATCCAGTT
	Reverse	AGGGAAGGCCGTGGTTGT
mCh313	Forward	AGAAGGGAGTTTCAAACCTGGT
	Reverse	GTCTTGCTCATGTGTGTAAGTGA
mMgl2	Forward	TTAGCCAATGTGCTTAGCTGG
	Reverse	GGCCTCCAATTCTTGAAACCT
mArg1	Forward	CTCCAAGCCAAAGTCCTTAGAG
	Reverse	AGGAGCTGTCATTAGGGACATC
mHPRT	Forward	TTGCTCGAGATGTCATGAAGGA
	Reverse	AGCAGGTCAGCAAAGAACTTATAGC
h18s	Forward	TCAACTTTCGATGGTAGTCGCCGT
	Reverse	TCCTTGGATGTGGTAGCCGTTTCT
mCyp2e1	Forward	TTCCCTAAGTATCCTCCGTGA
	Reverse	CGTAATCGAAGCGTTTGTTG
m16s rRNA	Forward	CCGCAAGGGAAAGATGAAAGAC
	Reverse	TCGTTTGGTTTCGGGGTTTC
mHexokinase 2	Forward	GCCAGCCTCTCCTGATTTTAGTGT
	Reverse	GGGAACACAAAAGACCTCTTCTGG
m18s	Qiagen	cat. number QT02448075

Table S2. List of antibodies used in Western blotting

Antibody name	Catalog number	Company	Isotype	Dilution
β-actin	4967	Cell Signaling Technology	Rabbit	1:1000
p-AKT (Ser473)	4060	Cell Signaling Technology	Rabbit	1:2000
t-AKT	9272	Cell Signaling Technology	Rabbit	1:1000
p-IRS1 (Tyr608) mouse/ (Tyr612) human	09-432	Millipore	Rabbit	1:1000
CD11c	97585	Cell Signaling Technology	Rabbit	1:1000
F4/80	70076	Cell Signaling Technology	Rabbit	1:1000
FAS	3180	Cell Signaling Technology	Rabbit	1:1000
P-JNK (Thr183/Tyr185)	4668	Cell Signaling Technology	Rabbit	1:1000
T-JNK (SAP/JNK)	9252	Cell Signaling Technology	Rabbit	1:1000
Phospho-eIF2α (Ser51)	9721	Cell Signaling Technology	Rabbit	1:1000
P-ERK (p44/42)	4695	Cell Signaling Technology	Rabbit	1:1000
IκBα	4812	Cell Signaling Technology	Rabbit	1:1000
LC3 I/II	2775	Cell Signaling Technology	Rabbit	1:1000
ACC	3676	Cell Signaling Technology	Rabbit	1:1000
PPARγ	81B8	Cell Signaling Technology	Rabbit	1:1000
VDAC1	4661	Cell Signaling Technology	Rabbit	1:1000
PDH	3205	Cell Signaling Technology	Rabbit	1:1000
GAPDH	Sc-137179	Sana Cruz Biotechnology	Mouse	1:500